Optical Pump-Probe Thermoreflectance Imaging for Anisotropic Heat Diffusion

Kazuaki Yazawa[*+], Jesús Armando León Gil[&], Kerry Maze[+], Dustin Kendig[*], and Ali Shakouri[+]
[*]Microsanj LLC.,
[&]Advanced Materials Research Center (Cimav),
[+]Purdue University
3287 Kifer Rd.
Santa Clara, California, USA, 95051
Email: info@microsanj.com

ABSTRACT

Thermal diffusion in anisotropic and inhomogeneous materials are investigated by full-field thermal imaging using optical pump-probe thermoreflectance microscopy. Target sample material is a composite of nickel clusters, approximately 10 microns in size, distributed inhomogeneously within polydimethylsiloxane (silicone) resin. Such a material presents special challenges when characterizing thermal parameters. For example, the nickel clusters are similar in size to the optical excitation spot size when performing ultra-fast time domain thermoreflectance measurement. This introduces uncertainty as to whether one is measuring the material average response over areas larger than the embedded metal clusters, or the local response of individual clusters. The proposed optical pump probe imaging method can separate material average (macroscopic) and local (microscopic) properties by characterizing sample surface temperature change over both large and small excitation and probe regions.

Experimental measurements are compared to both an analytic heat spreading model and finite element numerical simulation. Material anisotropy in the analytic solution is modeled using a well-known effective thickness method, which shows good agreement with the numerical simulation. Results suggest the proposed characterization method and associated analytical solution are applicable for thin or film-like materials with inhomogenous internal composite distribution and anisotropic thermal conductivity.

KEY WORDS: thermoreflectance, thermal diffusion, spreading resistance, inhomogeneous, Gaussian profile, laser spot.

NOMENCLATURE

a	heat spot diameter, m
b	length of spreading area, m
d	thickness, m
k	thermal conductivity, $W.m^{-1}.K^{-1}$
h	heat transfer coefficient, $W.m^{-2}.K^{-1}$
T	temperature, K

Greek symbols

Φ	spreading factor, (-)
λ	geometric factor, (-)
Ψ	dimensionless thermal resistance, (-)
σ	standard deviation

INTRODUCTION

Recent advancement in nano materials allows some composites of largely different material species to achieve unique characteristics. Our specific interest is in a polymer material with inhomogeneously embedded metal particles. We investigated a thick (500 microns thick) film of Polydimethylsiloxane (PDMS), also called silicone, compound with nickel (Ni) flake particles embedded to volumetric ratio of 20%. The material is inhomogeneous at length scales smaller than the size of the embedded Ni particle clusters, approximately 10 microns. Two versions of the Ni-polymer matrix are considered: a sample with randomly disordered Ni clusters and a sample with Ni clusters oriented in closely aligned chains oriented normal to the surface (cross-plane). The first sample is effectively isotropic (at length scales greater than the Ni clusters) while the second exhibits anisotropic properties with distinct in-plane and cross-plane electrical and thermal conductivities. [**Error! Bookmark not defined.**]. Thermal characterization has already been done for anisotropic materials with pump-probe method. However, this scale of inhomogeneity was not expected in the previous work. This report focuses on the understanding of heat diffusion in anisotropic and inhomogenous film materials with experiments, simplified analytic calculation, and numerical modeling.

MODEL

Analytical expression of the three-dimensional heat diffusion for our case is derived from literature with the resulting temperature distribution found by solving Bessel function [1] or Green's function [2]. However, we only need to perform a quick calculation result to set a proper condition for the characterization. A coarse estimate of the steady-state temperature distribution is more than helpful. A closed formula [3] was reported for the electronics cooling problems and is also useful to determine suitable conditions for the measurement of highly anisotropic materials. We used a scaling technique for through-plane heat conduction. An effective thickness d_{eff} adjusted with the ratio the anisotropy of thermal conductivity since the model uses only uniform thermal conductivity. This simple approach will be later supported by numerical solution by finite element method (FEM).

According to Ref. 3, heat spreading from the spot size *a* to the spreader size *b*, the non-dimensional thermal resistance of the peak (at the center) and the average of the range of the heating spot are formulated as,

$$\Psi_{max} = \frac{1}{\sqrt{\pi}}(1-\epsilon)\Phi \; and \; \Psi_{ave} = \frac{1}{2}(1-\epsilon)^{2/3}\Phi \qquad (1)$$

where, the factor Φ is found as a function of $\epsilon = a/b$. Bi is Biot number based on the spreader size, effective heat transfer coefficient h and thermal conductivity k of the spreader.

$$\Phi = \frac{\tanh(\lambda\tau)+\frac{\lambda}{Bi}}{1+\frac{\lambda}{Bi}\tanh(\lambda\tau)}, \text{with } \lambda = \pi + \frac{1}{\sqrt{\pi}\epsilon} \quad (2)$$

where, $\tau = d/b$ with spreader thickness d. Hence the thermal resistance ratio in respect to the peak is derived as,

$$\Psi_0 = \frac{\Psi_{ave}}{\Psi_{max}} = \frac{\sqrt{\pi}}{2(1-\epsilon)^{1/3}} \quad (3)$$

Since ϵ only relates to the spot size a,as the sample size is fixed, the normalized temperature profile at the spot edge is predicted to be independent of the anisotropy of the material. Following figure shows the expected temperature change per unit power (in mW) at the area of laser spot for various materials, including the properties and thicknesses of the sample materials discussed in our measurement. A 2 cm thick copper block is used as a heat sink for the film sample. Laser optical power is range of 10-50 mW.

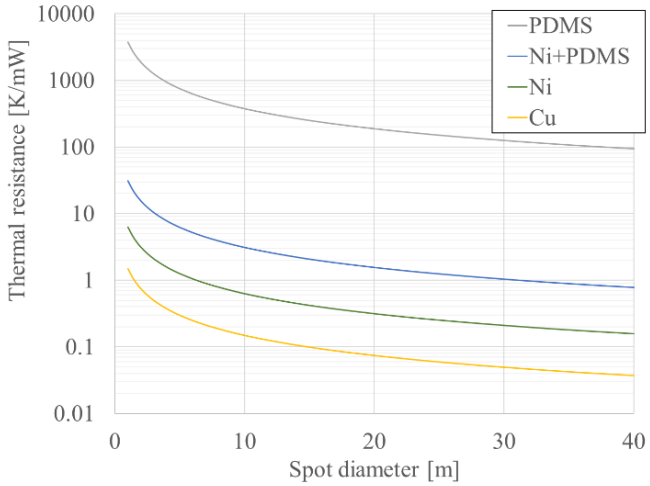

Fig. 1 Thermal resistance estimated for isothermal and homogeneous materials.

EXPERIMETAL METHOD AND APPARATUS

Photothermal measurement of thermal parameters

Several experiment methods have been developed to measure bulk and thin film thermal parameters such as thermal conductivity and thermal interface resistance. Many of these methods can be configured to measure anisotropic thermal properties. Photothermal approaches are popular due to being noncontact and highly configurable, allowing measurement of material thermal parameters over a wide range of sample types, spatial dimensions, and excitation frequencies. Photothermal measurement is based on temperature dependent changes in the optical properties of the subject material. Nearly all photothermal methods are based on a pump-probe apparatus which perturbs the sample thermally with a laser and measures the resulting temperature change. Infrared radiometry [4,5] excites a region of the sample with a laser (~ 40 um radius) and measures the resulting change in sample radiation with an infrared point detector. Photothermal lensing ('mirage') methods measure deflection of a probe beam through the heated region of sample, with the amount of deflection determined by the temperature dependent curvature [6,7] or gradient [5, 8,9] in index of refraction. Laser pump-probe thermoreflectance measures temperature dependent reflectance change in the ultra-fast time domain [10,11,12] or frequency domain [13]. Photothermal microscopes [14, 15,16] offer pump-probe measurement in compact experiment configurations.

Many of the experiment techniques mentioned can be adapted to measure anisotropic properties. Cross-plane and in-plane conductivity can be separated by changing the size of the pump spot, offsetting the location of the pump and probe spot, or changing the pump modulation frequency. In-plane anisotropy can be measured by scanning the pump along different surface axes (X-Y).

Optically pumped thermoreflectance imaging microscopy

Here we introduce optically pumped thermoreflectance imaging microscopy (OTI) as a method to rapidly extract material thermal parameters on both the macroscale and microscale. OTI builds on the principle of photoreflectance microscopy [16,17] by taking advantage of modern high signal to noise scientific grade CCD cameras. As in photoreflectance microscopy OTI excites a spot location on the sample surface using a pump laser. However instead of probing temperature change only at single points using a laser spot and photodiode, OTI simultaneously measures surface temperature change over the full microscope field of view by illuminating the sample with an LED probe source and recording the 2D probe response with a camera. The result is a rapid two-dimensional map of surface temperature change in response to the optical pump. As we show later, the spatial temperature distribution in the image can be analyzed to estimate thermal conductivity for both isotropic and anisotropic samples.

Fig. 2 shows the experiment configuration for optically pumped thermoreflectance imaging microscopy. Microscope, excitation and acquisition hardware and system software is based on a Microsanj thermoreflectance imaging system. By default, thermoreflectance microscopes excite the sample electrically. For optically pumped thermoreflectance microscopy this electrical source is replaced by an optical source, in this case an 825 nm diode laser that is coupled into the microscope and focused to a spot on the sample surface. Probe illumination is provided by a monochromatic LED centered at 530 nm, which illuminates the microscope full field of view. Both pump and probe are at normal incidence to the sample surface. The change in a material's reflectance with temperature is typically very small in the order of ~10^{-3} to 10^{-5}. Consequently, thermoreflectance measurements require lock-in amplification in some variation. Our configuration uses pulsed boxcar averaging in which both pump and probe are pulsed and synchronized. This approach not only enables temperature measurement with high resolution (10 millikelvin resolution), but also allows the thermal transient to be measured with 50 nanosecond temporal resolution. The spatial resolution of the resulting temperature image is also diffraction limited, or ~ 250 nm. The minimum size of the pump spot is determined by the

diffraction limit for a given objective numerical aperture. At 100X magnification (NA = 0.75) the full width at half maximum (FWHM) of the laser spot was 400 nm. The corresponding field of view of the sample surface in the image at this magnification is approximately 80 microns. Thermal response for larger pump spots and over a larger region of the sample can quickly be inspected by decreasing objective magnification. This is useful for comparing macroscopic and microscopic material thermal properties, which we demonstrate in this paper.

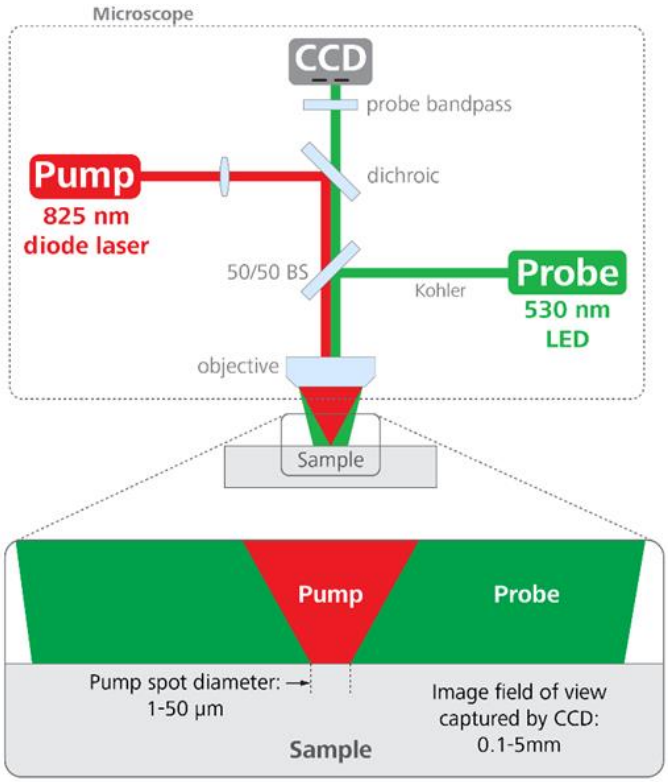

Fig. 2 Experiment configuration for optically pumped thermoreflectance imaging microscope.

Measuring submicron heat distribution

At length scales, much greater than the size of underlying inhomogeneities in a matrix, the material can be treated as effectively homogenous. This is represented by the macroscopic OTI images of the Ni-PDMS at low magnification (5X). However, at microscopic length scales the Ni-PDMS cannot be considered effectively homogenous. At these lengths nickel clusters (~ 20 microns in diameter) form discrete bodies in an inhomogeneous mixture. Thermal transport at this submicron length scale is governed by local interaction between neighboring nickel clusters within the PDMS matrix. Consequently, temperature distribution in the Ni-PDMS at the microscopic scale is strongly influenced by the relative order or disorder of the nickel clusters. Microscopic thermal transport can be inspected by performing OTI at high magnification. Fig. 3 shows top view optical and thermoreflectance microscope temperature change images for isotropic (unaligned) and anisotropic (aligned) Ni-PDMS samples. Magnification is 100X and NA = 0.75. Diffraction limited spatial resolution is 300 nm. The effect of magnetic alignment on the nickel clusters visible in the optical images. Nickel clusters (the bright features) in the unaligned (isotropic) sample are distributed randomly both laterally and into the depth of the polymer (dark region). In the aligned (anisotropic) case the nickel clusters are ordered vertically along the sample, normal to the imaging axis, and only a single topmost nickel cluster is visible on the surface. At this magnification, the pump spot can be focused to a radius of 400 nm, which permits excitation of individual nickel clusters. The optical images in Fig. 3 show the location of the pump spot and corresponding excited discrete nickel cluster on the sample surface. Incident pump power is 10 mW. The thermal images show heat diffusion for both isotropic and anisotropic cases, calibrated for temperature change along the surface of the polymer. In the isotropic sample temperature distribution is highly asymmetric, conforming spatially to the arrangement of nickel clusters that adjoin or neighbor the excited cluster. This can be interpreted as heat diffusing through local microscopic domains of increased thermal conductance where the highly conductive nickel clusters are more concentrated. In contrast temperature distribution in the anisotropic sample displays highly radial symmetry, consistent with the columnar alignment of nickel cluster into the depth of the sample. This characteristic was confirmed for measurements at three locations for both samples.

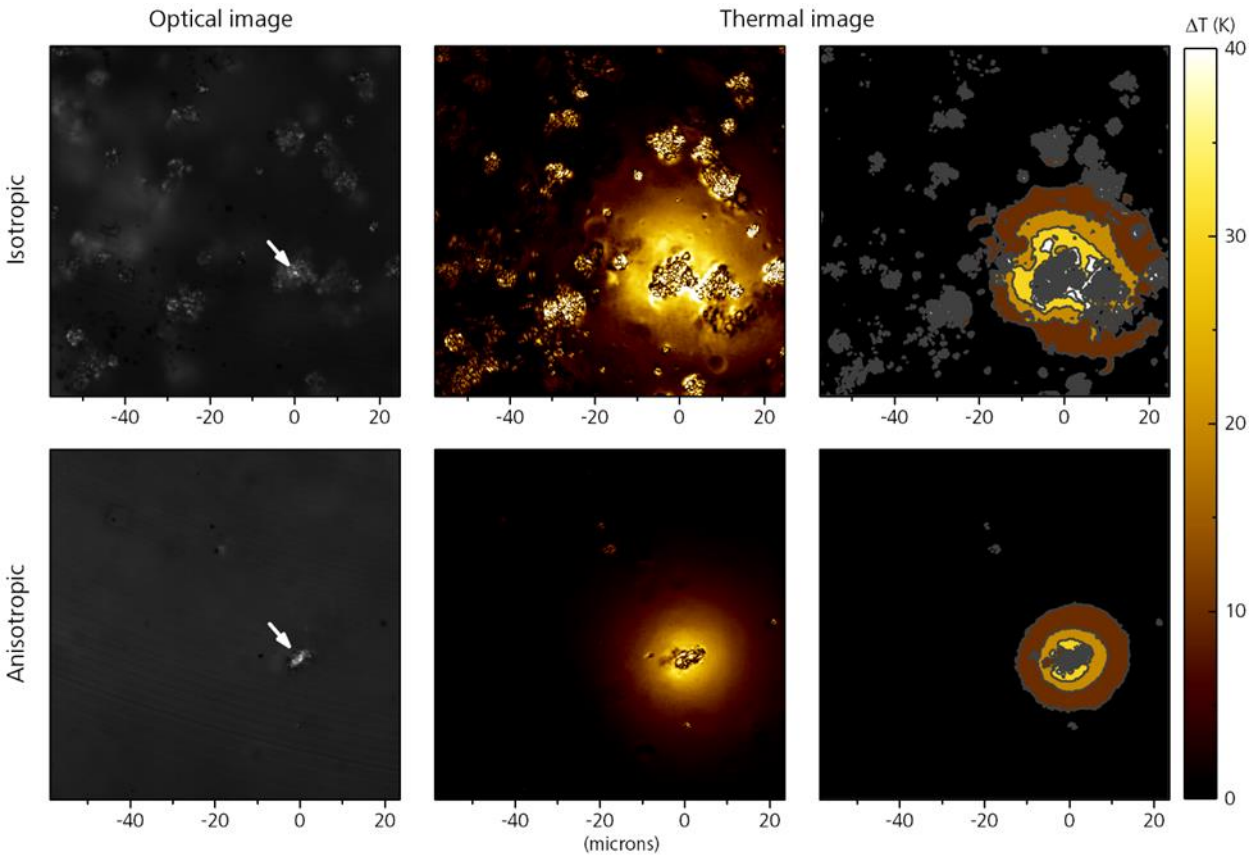

Fig. 3 Microscopic heat transport in the Ni-PDMS. Top view Submicron resolution (100X) OTI optical and thermal images of isotropic and anisotropic Ni/PDMS samples. Pump spot (arrows) radius is 400 nm. Incident pump power is 10 mW. Light features in optical image are nickel clusters, dark regions are polymer. Thermal images are calibrated to show temperature change distribution in polymer region.

RESULTS AND DISCUSSIONS

The employed samples for this study consists in two different films which are compound materials based on PDMS as matrix with 20%wt of nickel particles embedded. Fabrication of these films is done by a roll-to-toll (R2R) process that applies an external magnetic field to align the particles inside the flexible matrix. Using this technique is possible to highly orientate the Ni particles in the thickness direction providing anisotropic features along this axis [18]. Therefore, to demonstrate the capabilities of the Optical Thermoreflectance Imaging technique for measuring anisotropic heat diffusion we compare the heat transfer response between a non-aligned and an aligned Ni/PDMS samples.

To verify the anisotropic heat diffusion, we explored experimentally the heat transfer phenomenon in two different polymer samples using the OTI imaging technique at macroscopic scale (5X). Since at this magnification the effective medium of each sample should vary due to the different organization of the Ni particles inside the polymer matrix. Furthermore, the polymer presents low thermal conductivity (0.15 $W.m^{-1}.K^{-1}$) hence the need of a slow square pulse of 2 ms to guarantee samples heating. Images were average for 30 min. The thermoreflectance image was calibrated for temperature change using experimentally obtained thermoreflectance coefficient, measured at the probe wavelength of 530 nm. The thermoreflectance coefficient for the isotropic polymer sample -2.1×10^{-3} K^{-1}. Fig. 4(a)-(d) illustrates the CCD and the thermal images for both compounds films, the anisotropic/aligned and isotropic/non-aligned Ni/PDMS samples, at 5X of magnification displaying the pump spot size and the resulting heat distribution, elucidating significant heat distribution for both samples. Therefore, in behalf of demonstrating the capabilities of this novel technique a comparison of temperature profiles between the polymer compounds is carried out, the results are shown in Fig. 5.

To analyze the thermal images and the heat spreading for both cases a numerical analysis method is performed. For this numerical analysis, the raw data is subtracted from the thermal image as a matrix data arrangement. Then, using MATLAB a low-pass FFT filter is applied in pursuance of reducing noise that could be present in the data. During FFT filter a cutoff frequency is defined to exclude the noise. Then, using the processed data a two-dimensional Gaussian model is fitted with the objective of finding the center of heat spot. Once the peak center is known a temperature profile is taken, due to rotation and interpolation of the image it is possible to acquire more profiles at different angles along the radius of the heat

distribution and finally average them. Because of the signal-to-noise ratio increment is possible to elucidate that the OTI imaging technique is capable of measuring heat distribution anisotropy. Nevertheless, there still some noise inherent to the experimental setup.

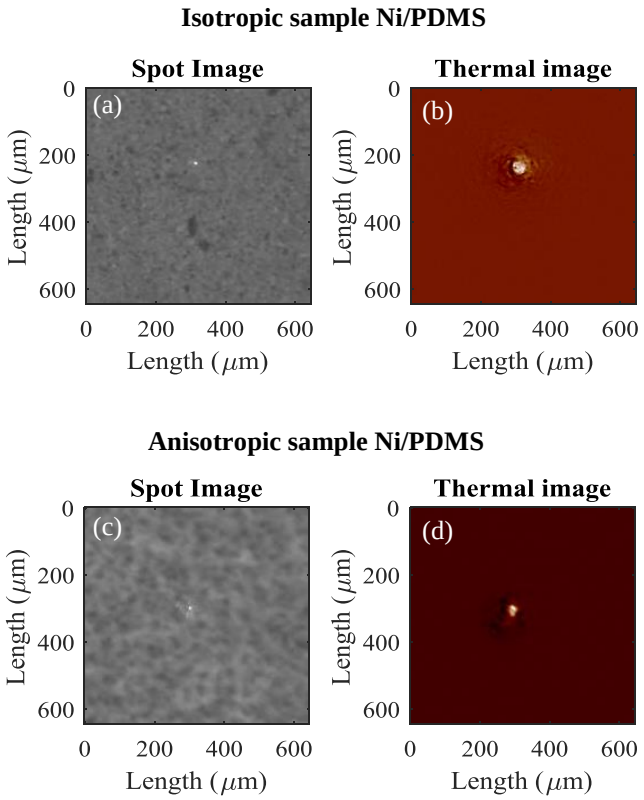

Fig. 4 Experimental data obtained from OTI technique: (a) Isotropic Ni/PDMS spot size image, (b) Isotropic Ni/PDMS thermal image, (c) Anisotropic Ni/PDMS spot size image, (d) Anisotropic Ni/PDMS thermal image.

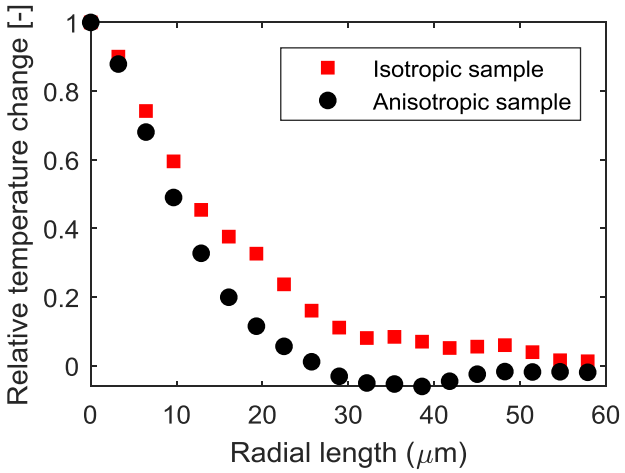

Fig. 5 Temperature profiles obtained from the numerical analysis with MATLAB.

Alternatively, heat transfer FEM simulations were performed using Ansys Workbench where the compounds films are considered as two different effective mediums. Fig. 6(a) shows an example illustrating FEM arrangement placing a Cu heat sink under the polymer film. The meshed structure utilized for pump spot has a minimum element size 0.5 µm, compound films and heat sink have 40 µm and 60 µm maximum element size, respectively. Total absorbed power at the spot location was estimated at approximately 10 mW. The heat load applied is considered to have a Gaussian distribution. Therefore, in order to obtain this Gaussian pulse, the incident pump spot was composed of three sections with a radius of 7 µm, 15 µm, 30 µm with 68%, 26% 4.2% of the total power, respectively. Resultant heat distribution is displayed in Fig. 6(b). Properties for the isotropic element are defined taking in consideration the weight percentage of each material (20% Ni/80% PDMS). Regarding thermal conductivity (k), which is the property of interest, literature reports a value of 0.15 $W.m^{-1}.K^{-1}$ for PDMS [19] and a well-known value of 90 $W.m^{-1}.K^{-1}$ is used for Ni giving a resultant k for the isotropic effective medium of 18.1 $W.m^{-1}.K^{-1}$. Additionally, anisotropic heat distribution is taken into consideration by defining k in terms of tensors. Simplifying the model thermal conductivity is only considered in xx, yy and zz tensor components of the local Cartesian coordinate where k_{zz} is equal to or larger than k_{xx} and k_{yy} ($k_{xx} = k_{yy}$). Fig. 7 shows a comparison between isotropic and anisotropic compounds films evaluating the latter film as a function of different thermal conductivity (k) values in its tensor components.

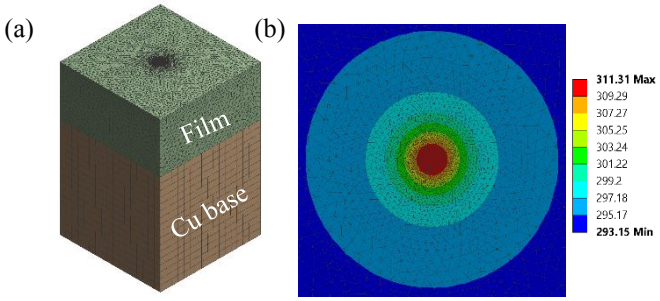

Fig. 6 (a) FEM meshing model in ISO view and (b) result temperature contour from top view of the film. The mesh density at the center spot is significantly large compared to the surrounding area.

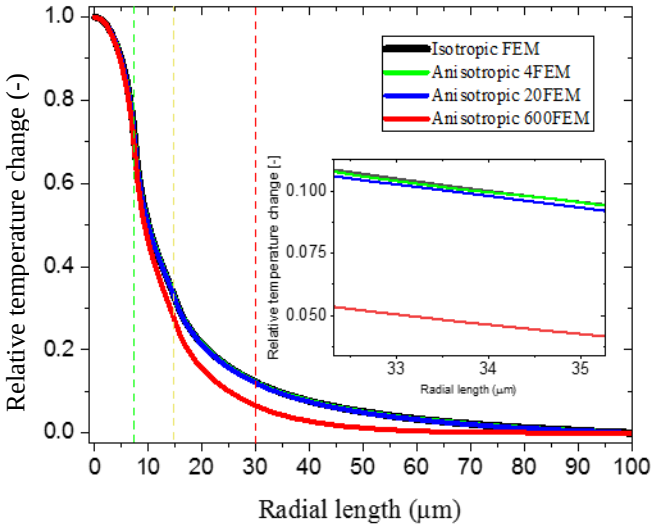

Fig. 7 Temperature profiles estimated for the isotropic and anisotropic samples where thermal conductivity properties for the anisotropic medium are being varied. Vertical dash lines show the spot radius green (7 μm), yellow (15 μm) and red (30 μm). Zoomed rectangular shows the changes in relative temperature varying by anisotropy factor 4, 20, and 600.

Thermal properties used in FEM simulation remain unchanged for the isotropic Ni/PDMS sample. On the other hand, anisotropic case first evaluation is performed using $k_{xx} = k_{yy} = 18.1$ W.m^{-1}.K^{-1}. Meanwhile, $k_{zz} = 80$ W.m^{-1}.K^{-1} making the film 4 times more conductive along the z-axis. As can be seen from the inset in Fig. 7 anisotropy is very small. One possibility is that when the Ni particles are aligned along thickness direction may also decrease k in x and y components. Taking that into account for a second calculation k is decreased for a factor 4.4 as well giving a $k_{xx} = k_{yy} = 4.1$ W.m^{-1}.K^{-1}. The outcome for k_{zz}/k_{xx} ratio increases to 20. Additional curve exhibits an extreme case defining $k_{xx} = k_{yy} = 0.15$ W/m/K and $k_{zz} = 90$ W.m^{-1}.K^{-1} what corresponds to k original values of PDMS and Ni, respectively, resulting in a k_{zz} / k_{xx} ratio of 600.

Fig. 8(a)-(b) shows the FEM result contour. Note that the depth scale was adjusted to compare the profile, which are compensating the anisotropy. Elucidating a higher heat spreading along the z-axis and significantly narrower. Fig. 8(c) shows the comparison between experimental and FEM results. FEM results corresponds to extreme case where the $k_{zz} / k_{xx} = 600$. As seen in Fig. 8(c), the heat spot radius is outlined at 7 μm with green vertical line, 15 μm with yellow line and 30 μm with red line. Note that the general characteristics of the temperature profile is relatively in agreement as the profile is taken inside the heat spot length except for the outer section. Moreover, the FEM results also show that the profile is very insensitive to the change in anisotropy, where experimental profile seems to reflective larger difference in slope. This discrepancy is related to the samples nature which exhibit roughness at the surface. For example, this occurrence is clear for the anisotropic sample which shows a relative temperature change below zero at radial length of 30-40 μm. similarly, noisy profile shape is shown for the isotropic sample at this region too.

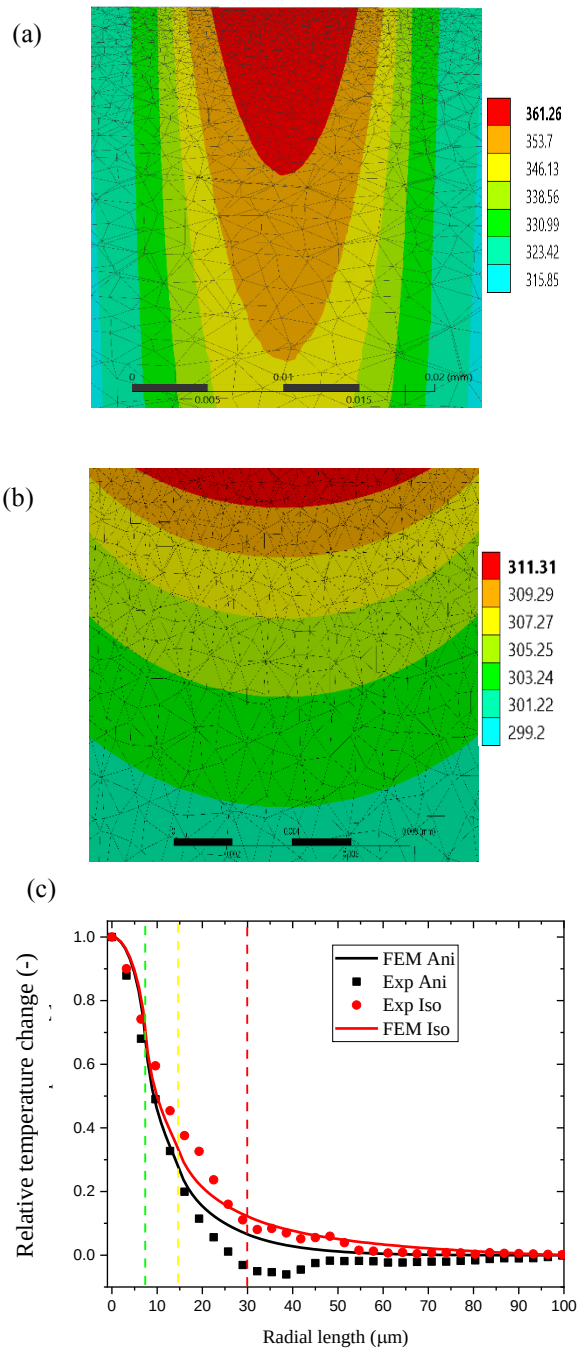

Fig. 8 (a) Cross-plane section of anisotropic Ni/PDMS, (b) Cross-plane section of isotropic Ni/PDMS (c)Heat distribution comparison of isotropic and anisotropic Ni/PDMS experimental results and FEM results. Anisotropic thermal conductivity: $k_{xx} = k_{yy} = 0.15$ W.m^{-1}.K^{-1} and $k_{zz} = 90$ W.m^{-1}.K^{-1}. Vertical dash lines show the spot radius green (7 μm), yellow (15 μm) and red (30 μm).

By fitting the normalized temperature by peak temperature T_0 with an assumption of Gaussian or Lorentzian profile, experimental results observe relatively closer to Lorentzian, while the numerical results are much closer to Gaussian. The Gaussian is generally expressed as,

$$T(r)/T_0 = \frac{1}{\sqrt{2\pi}\sigma}\exp\left\{-\frac{(x-x_0)^2}{2\sigma^2}\right\} \quad (4)$$

and Lorentzian is,

$$T(r)/T_0 = \frac{1}{\pi}\frac{\gamma}{(x-x_0)^2+\gamma^2} \quad (5)$$

where, σ is standard deviation of Gaussian distribution and γ is FWHM/2 of Lorentzian distribution. In this case, x_0 is zero because the temperature distribution considers the axisymmetric distribution along the Y-axis at x = 0.

Fig. 9 (a) and (b) show the analytic fitting against the previous shown FEM results in data points, which agreed well with the experimental results (Fig. 8). The FWHM values are 16.6 for Isotropic case and 15.5 for Anisotropic case, respectively taken from the experimental data with the minimum error. For both cases, Gaussian function did a better job in predicting the peak temperature profile at the region over the FWHM. The difference between two functions, however, was small and Lorentzian function fits much better in lower fillet profile. Hence, Lorentzian function would be adequate to describe the temperature excess profile. Lorentzian distribution known as Cauchy distribution has the mathematical background of deriving vibration resonance, which can be translated into a second-order differential equation. Since the heat diffusion equation has the same order, it is natural to assume that the profile of resonant amplitude could also represent the temperature profile, while the heat power is given at the center by optical pump. In this condition, the surrounding thermal boundary for this small circular spot is considered as the infinite medium. Hence the fillet profile has no strong constraint to pull down to the base temperature. Therefore, Gaussian profile is relatively inappropriate for this case.

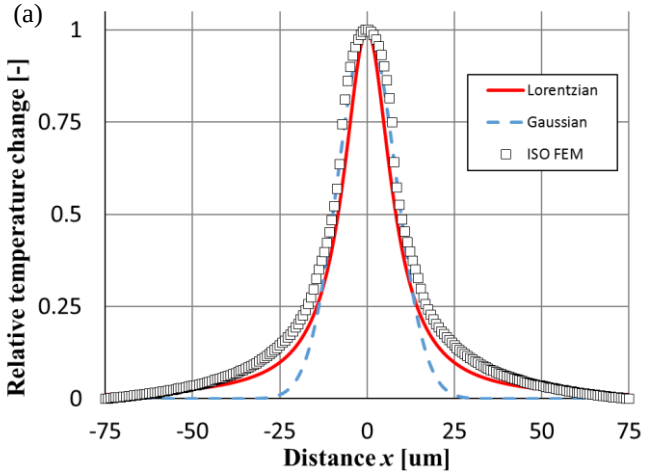

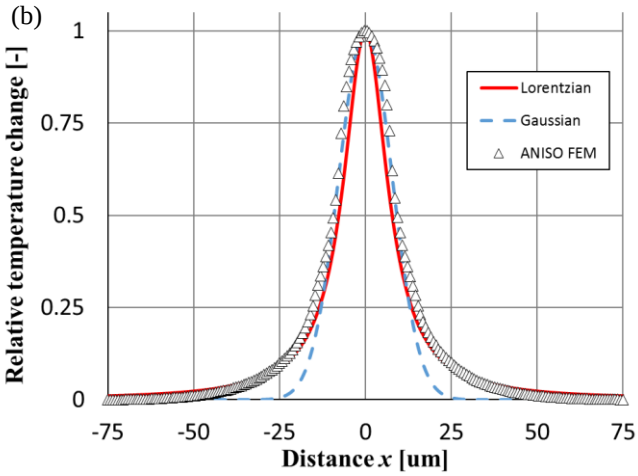

Fig. 9 Temperature profile comparison of analytic Gaussian and Lorentzian model with FEM results (data points) for (a) Isotropic case and (b) Anisotropic case.

CONCLUSIONS

Optical pump-probe thermoreflectance imaging is used to investigate the heat diffusion in the inhomogeneous and anisotropic film materials. The sample consists nickel particles in composite of Polydimethylsiloxane resin. Due to the flexible and relatively thin (500 um) material, a solid base copper heat sink is used to support.

Full three-dimensional numerical simulation shows a qualitative agreement in profile, but there are discrepancies observed nearby boundary of the laser spot as well as the lower profile. Internal heat diffusion profile in the film thickness looks quite like any anisotropy ratio as far as the effective thickness linearly compensates the anisotropy. The discrepancy of the fitting needs additional work that includes a numerical analysis with Gaussian power profile of laser input. According to the analytic fitting, Lorentzian (Cauchy) distribution function is rather appropriate than Gaussian to predict the temperature distribution for the optical pump method, where surrounding thermal boundary is far off compared to size of spot.

In the future work, we would extend this technique to multilayers and simple transistors, such as gallium nitride (GaN) high electron mobility transistors (HEMTs), to characterize the 'effective' anisotropic thermal structure of electronic devices.

References

[1] M. N. Ozisik, *Heat Conduction Second edition*, John Wiley, 1993.

[2] K. D. Cole, A. Haji-Sheikh, J. V. Beck, B. Litkouhi, *Heat conduction Using Green's Function Second Edition*, CRC Press, 2011.

[3] S. Lee, S. Song, V. Au, K. P. Moran, Constriction/Spreading Resistance Model for Electronics Packaging, Proc. ASME/JSME Thermal Engineering Conference: Vol. 4, ASME, pp. 199-206, 1995.

[4] J. Guitonny, G. C. Pandey, A. C. Boccara, and D. Fournier, "Thermal diffusivity measurement by I.R. microscopy:

application to opaque polymeric samples," Le Journal de Physique IV, vol. 04, no. C7, pp. C7-307-C7-309, Jul. 1994.

[5] A. Salazar, A. Sánchez‐Lavega, A. Ocariz, J. Guitonny, G.C. Pandey, D. Fournier, and A.C. Boccara, "Thermal diffusivity of anisotropic materials by photothermal methods," Journal of Applied Physics, vol. 79, no. 8, p. 3984, 1996.

[6] J. R. Whinnery, "Laser measurement of optical absorption in liquids," Accounts of Chemical Research, vol. 7, no. 7, pp. 225–231, Jul. 1974.

[7] J. Rantala, J. Jaarinen, and P. K. Kuo, "The effects of experimental parameters in the thermal diffusivity measurements of oriented polymer films using mirage effect: computer simulation," Applied Physics A: Materials Science & Processing, vol. 55, no. 6, pp. 586–595, 1992.

[8] W. B. Jackson, N. M. Amer, A. C. Boccara, and D. Fournier, "Photothermal deflection spectroscopy and detection," Applied Optics, vol. 20, no. 8, p. 1333, Apr. 1981.

[9] C. Gan and X. Zhang, "Investigation of Anisotropic Thermal Diffusivity Using the "Mirage Effect"," In Photoacoustic and Photothermal Phenomena, pp. 335-338. Springer, Berlin, Heidelberg, 1988.

[10] A. J. Schmidt, X. Chen, and G. Chen, "Pulse accumulation, radial heat conduction, and anisotropic thermal conductivity in pump-probe transient thermoreflectance," Review of Scientific Instruments, vol. 79, no. 11, p. 114902, Nov. 2008.

[11] J. P. Feser and D. G. Cahill, "Probing anisotropic heat transport using time-domain thermoreflectance with offset laser spots," Review of Scientific Instruments, vol. 83, no. 10, p. 104901, Oct. 2012.

[12] P. Jiang, X. Qian, and R. Yang, "Time-domain thermoreflectance (TDTR) measurements of anisotropic thermal conductivity using a variable spot size approach," Review of Scientific Instruments, vol. 88, no. 7, p. 074901, Jul. 2017.

[13] D. Rodin and S. K. Yee, "Simultaneous measurement of in-plane and through-plane thermal conductivity using beam-offset frequency domain thermoreflectance," Review of Scientific Instruments, vol. 88, no. 1, p. 014902, Jan. 2017.

[14] L. Pottier, "Micrometer scale visualization of thermal waves by photoreflectance microscopy," Applied Physics Letters, vol. 64, no. 13, pp. 1618–1619, Mar. 1994.

[15] K. Plamann, D. Fournier, B. C. Forget, and A. C. Boccara, "Microscopic measurements of the local heat conduction in polycrystalline diamond films," Diamond and related materials, vol. 5, no. 6–8, pp. 699–705, 1996.

[16] B. Li, L. Pottier, J. P. Roger, D. Fournier, K. Watari, and K. Hirao, "Measuring the anisotropic thermal diffusivity of silicon nitride grains by thermoreflectance microscopy," Journal of the European Ceramic Society, vol. 19, no. 8, pp. 1631–1639, Jun. 1999.

[17] A.M. Mansanares, T. Velinov, Z. Bozoki, D. Fournier, and A. C. Boccara. "Photothermal Microscopy: Thermal Contrast at Grain Interface in Sintered Metallic Materials," Journal of Applied Physics 75, no. 7, pp. 3344–50, Apr. 1994..

[18] Y. Chen, Y. Guo, S. Batra, E. Unsal, E. Wang, Y. Wang, X, Liu, Y. Wang, and M. Cakmak, "Large-scale R2R fabrication of piezoresistive films (Ni/PDMS) with enhanced through thickness electrical and thermal properties by applying a magnetic field," RSC Advances, **5**(112), pp. 92071-92079, 2015.

[19] C. Livermore, J. Voldman, "6.777 J/2.751 J Material Property Database," 2004.